Fluorescence based dual sensor of Zn^{2+} & PO_4^{3-} and the application of soft computing methods to predict machine learning outcomes

Shashanka Shekhar Samanta[a], Subhadip Giri[a], Sourav Mandal[a], Usha Mandal[a], Hasibul Beg[b] and Ajay Misra[a*].

[a]Department of Chemistry, Vidyasagar University, Midnapore-721102, West Bengal, India.

[b]Department of Chemistry, Raja N. L. Khan Women's College, Midnapore, 721102, India.

Corresponding Author:

[*] Email: ajay@mail.vidyasagar.ac.in; Tel.: +91 8967986988; Fax: +91 3222 275329.

**Synthesis of phenolphthalein-di-aldehyde (A):**

A solution of phenolphthalein (0.955 g, 3 mmol) in trifluoroacetic acid (TFA) (25 mL) over ice was slowly added to hexamethylenetetramine (HMTA) (1.154 g, 8.24 mmol) and stirred for30 min at room temperature. Then the solution was refluxed in an oil bath for 12 h maintaining the temperature at 95 °C. After completion of the reflux, the reaction mixture was dried out in a rotavapor. A Reddish-brown colour liquid was obtained. Then chilled water was added to the liquid product. White colour precipitation was appeared, it was filtered and washed by water several times to free from acid. The solid product was subjected to column chromatography with 10:1 n-hexane-ethyl acetate to get pure product **A.** Yield ~74%; $C_{22}H_{14}O_6$ ^{1}H NMR (400 MHz, $CDCl_3$) δ 11.18 (s, 2H), 9.89 (s, 2H), 8.07 (d, J = 7.7 Hz, 1H), 7.85 (t, J = 8.1 Hz, 1H), 7.71 (t, J = 7.5 Hz, 1H), 7.63 (s, 1H), 7.62 (d, J = 2.4 Hz, 2H), 7.54 (dd, J = 8.8, 2.4 Hz, 2H), 7.08 (s, 1H), 7.06 (s, 1H) (Fig. S1), FT-IR (cm-1): 3365 (phenolic -OH), 2855 (H of aldehyde), 1759 (-COO-spirolactam ring), 1659 (-CHO) (Fig. S2). ESI-MS: calcd. 374.0790, obtained 375.1712 [M + H]$^+$(Fig. S3).
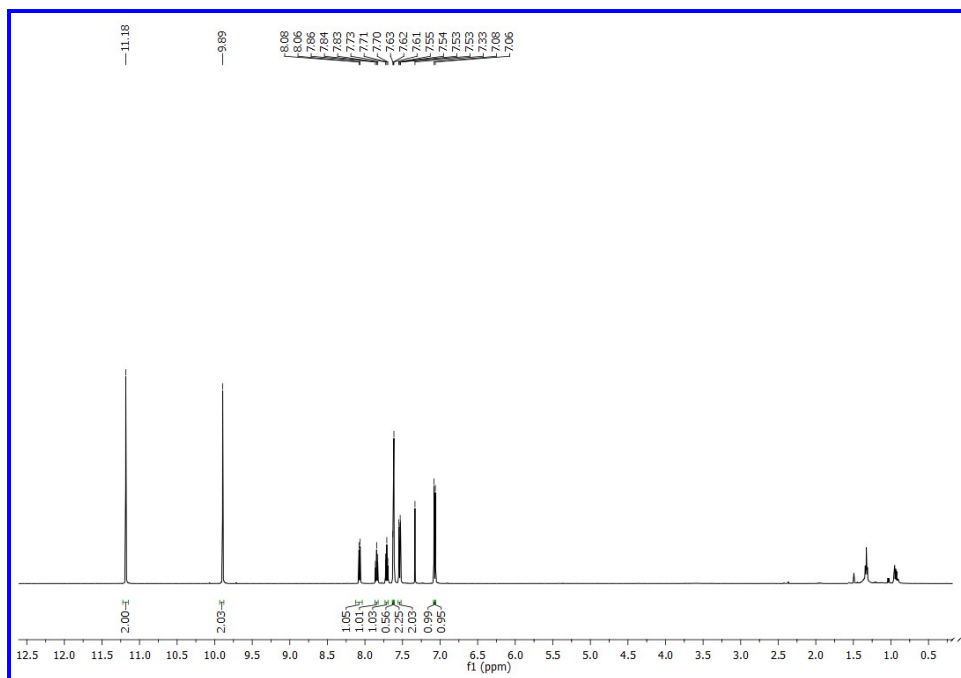
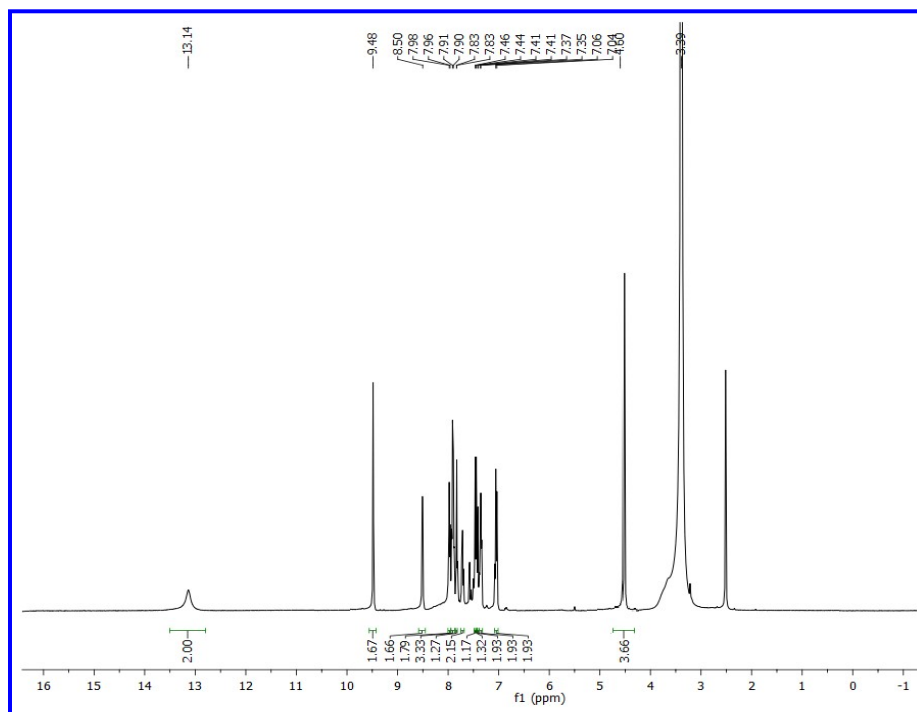**Fig. S1**: ^{1}H NMR data of 5,5'-(3-oxo-1,3-dihydroisobenzofuran-1,1-diyl)bis(2-hydroxy benzaldehyde (**A**) in CDCl$_3$ medium.
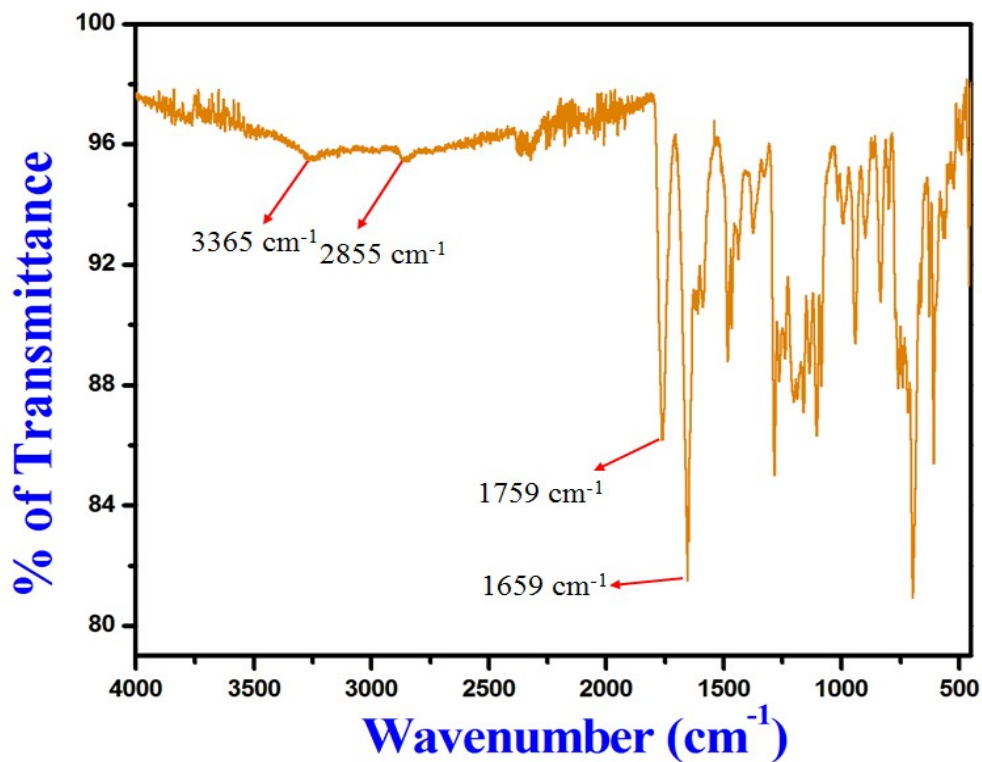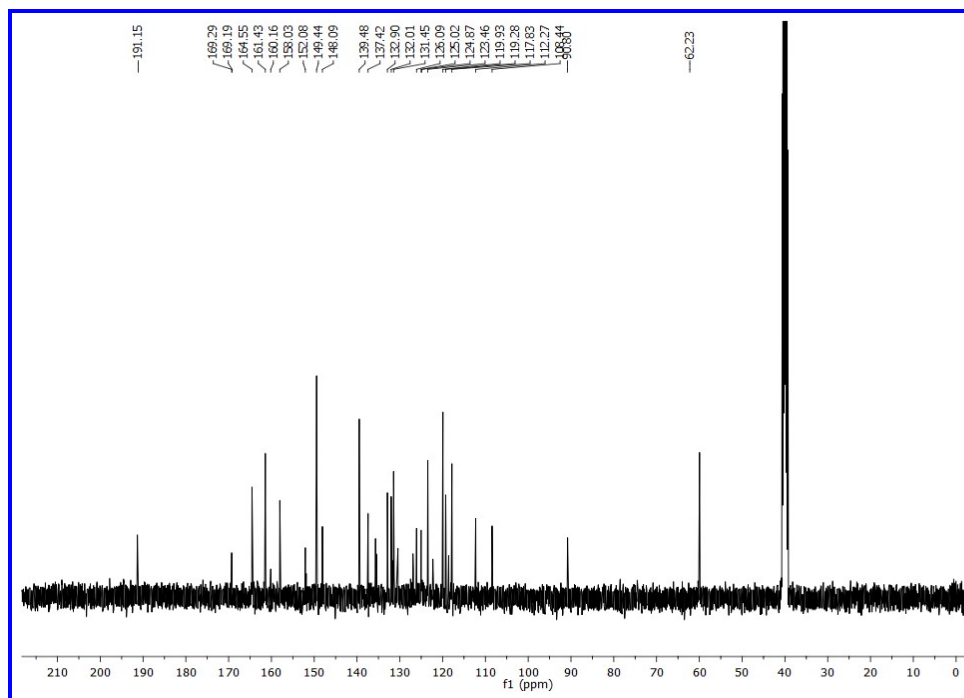

Fig. S2: FT-IR spectra of 5,5'-(3-oxo-1,3-dihydroisobenzofuran-1,1-diyl)bis(2-hydroxy benzaldehyde (**A**).
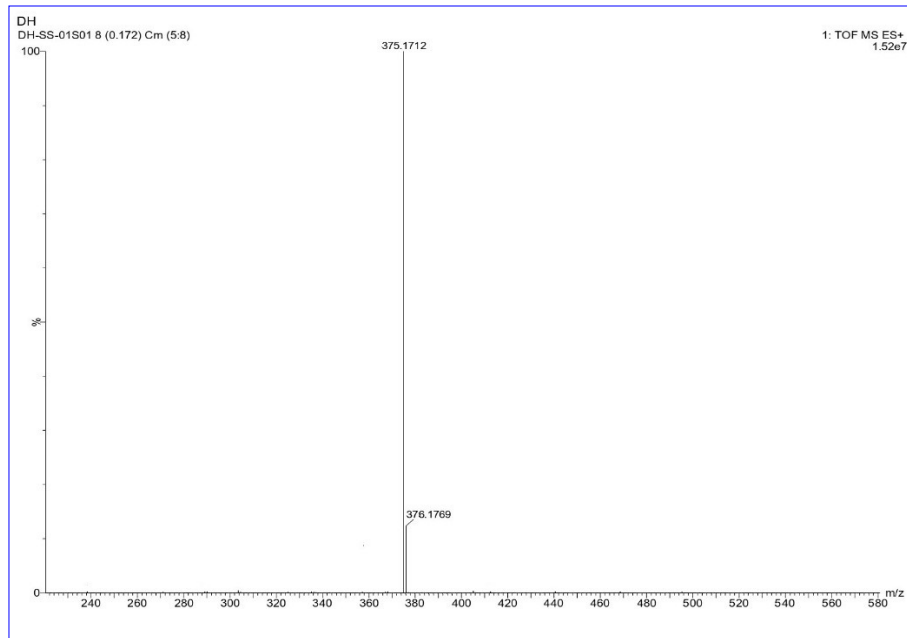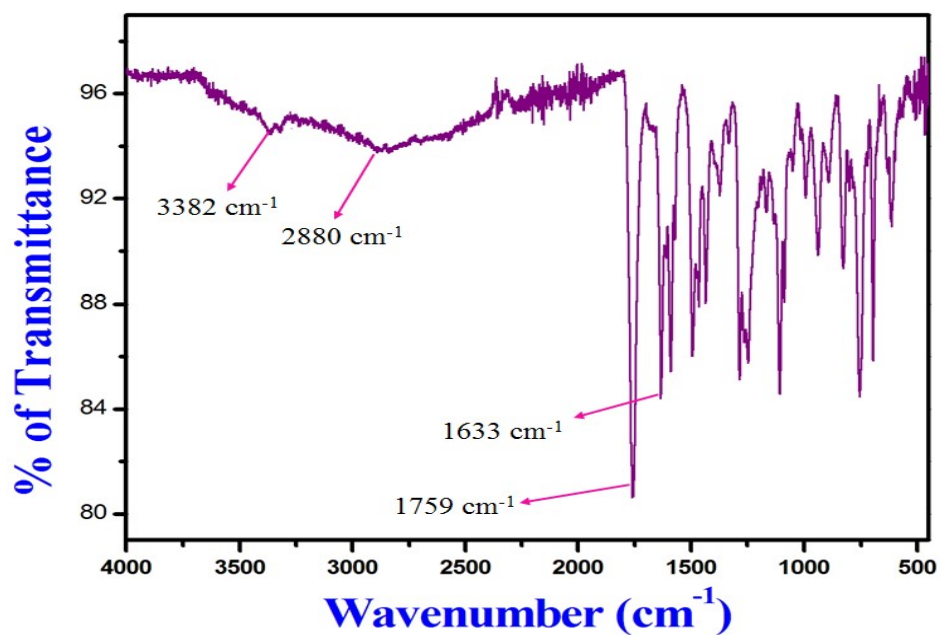
Fig. S3: ESI-MS data of 5,5'-(3-oxo-1,3-dihydroisobenzofuran-1,1-diyl)bis(2-hydroxy Benzaldehyde (**A**). [M+H]$^+$: 375.1712.

Fig. S4: ^{1}H NMR data of 3,3-Bis-{4-hydroxy-3-[(pyridine-2-ylmethylimino)-methyl]-phenyl}-3*H*-isobenzofuran-1-one (PAP) in DMSO-d$_6$.
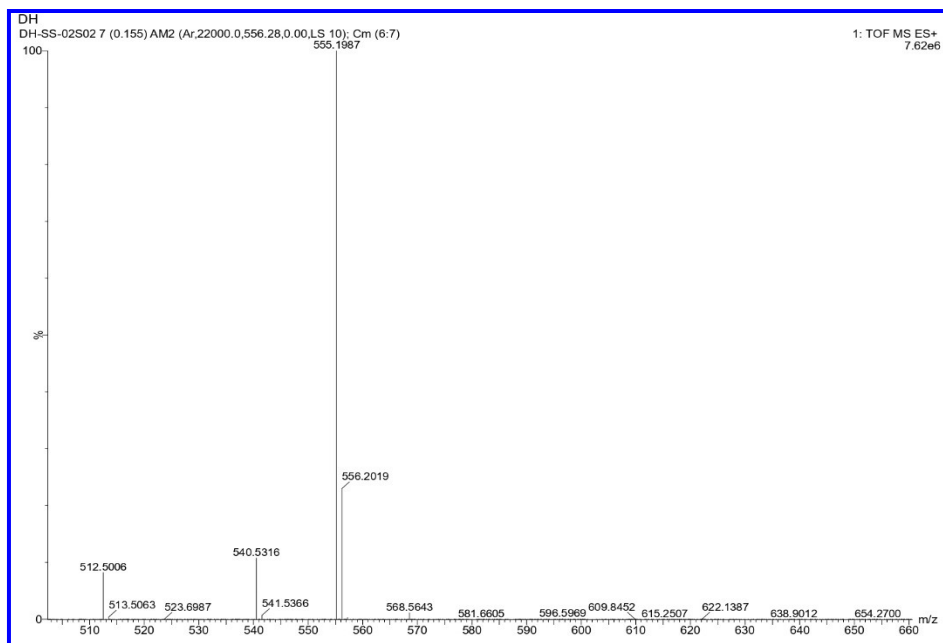
Fig. S5: ^{13}C NMR data of 3,3-Bis-{4-hydroxy-3-[(pyridine-2-ylmethylimino)-methyl]-phenyl}-3*H*-isobenzofuran-1-one (PAP) in DMSO-d$_6$.

Fig. S6: FT-IR spectra of 3,3-Bis-{4-hydroxy-3-[(pyridine-2-ylmethylimino)-methyl]-phenyl}-3*H*-isobenzofuran-1-one (PAP).

Fig. S7: ESI-MS data of 3,3-Bis-{4-hydroxy-3-[(pyridine-2-ylmethylimino)-methyl]-phenyl}-3*H*-isobenzofuran-1-one (PAP). [M+H]$^+$: 555.1987.
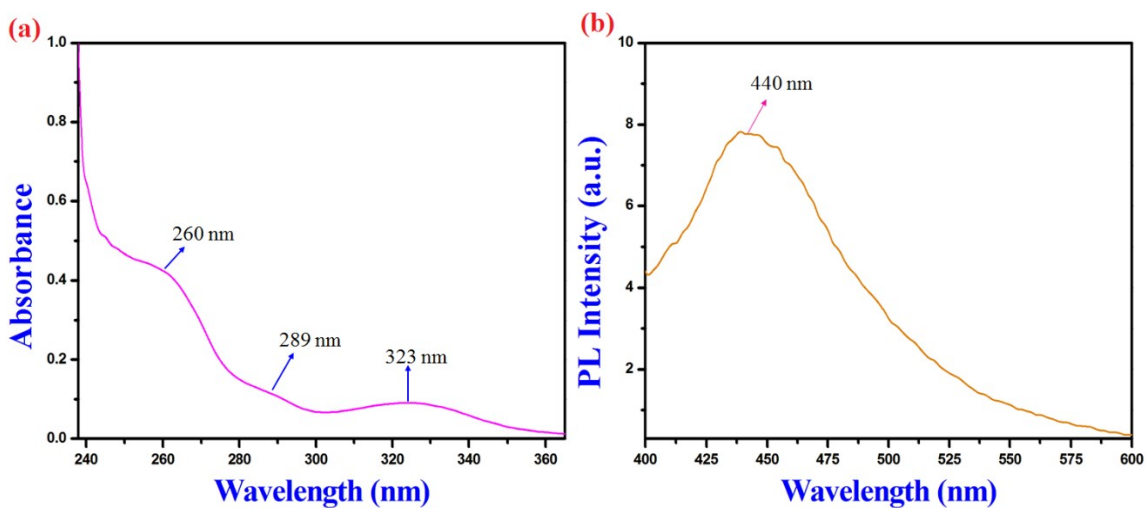
Fig. S8: (a) UV-Vis spectra of PAP; in THF medium, (b) Steady state emission spectra of PAP in THF (λ_{ex}: 350nm) (excitation/emission spectral band width: 5nm).
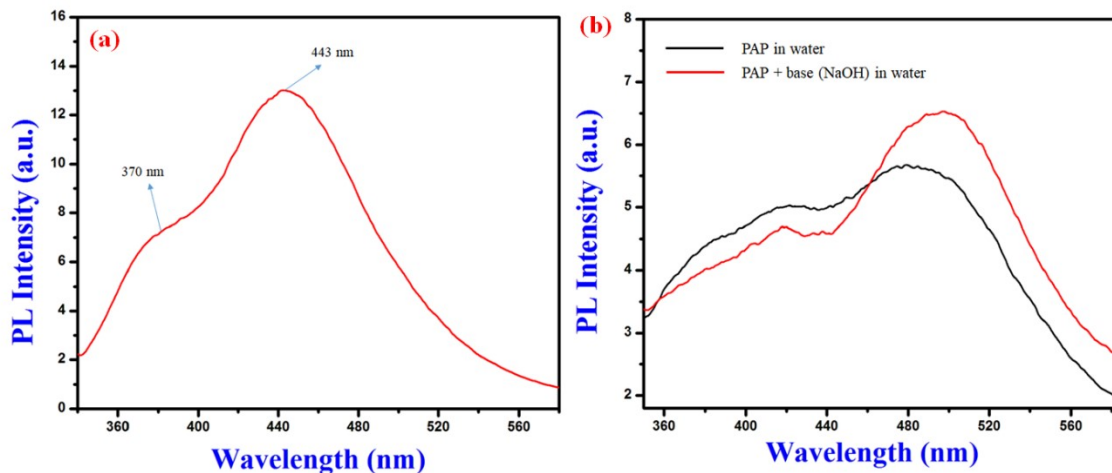
Fig. S9: (a) Emission spectra of PAP in THF medium upon 288 nm excitation, (b) Emission spectra of PAP in water and PAP with base (NaOH, 1 µM) in water upon 288 nm excitation.
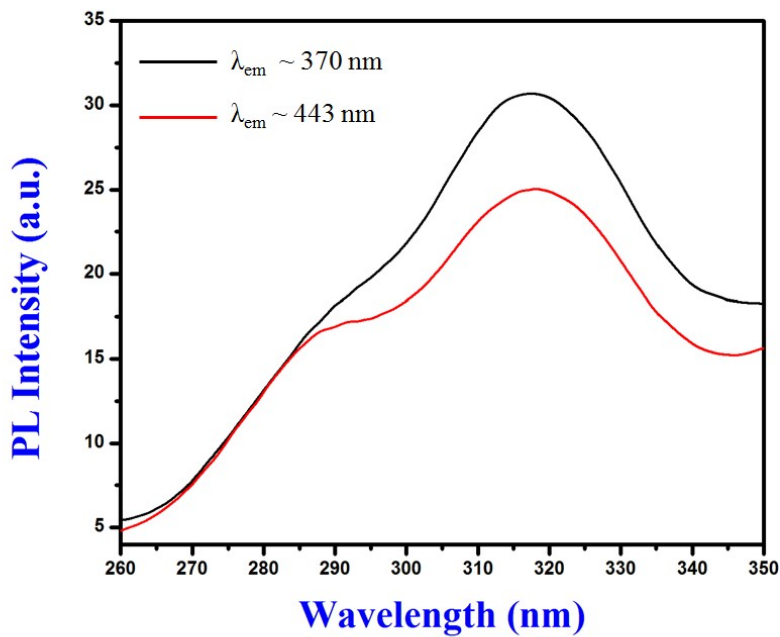
Fig. S10: Fluorescence excitation spectra of PAP in THF medium by monitoring at 370 nm and 443 nm.
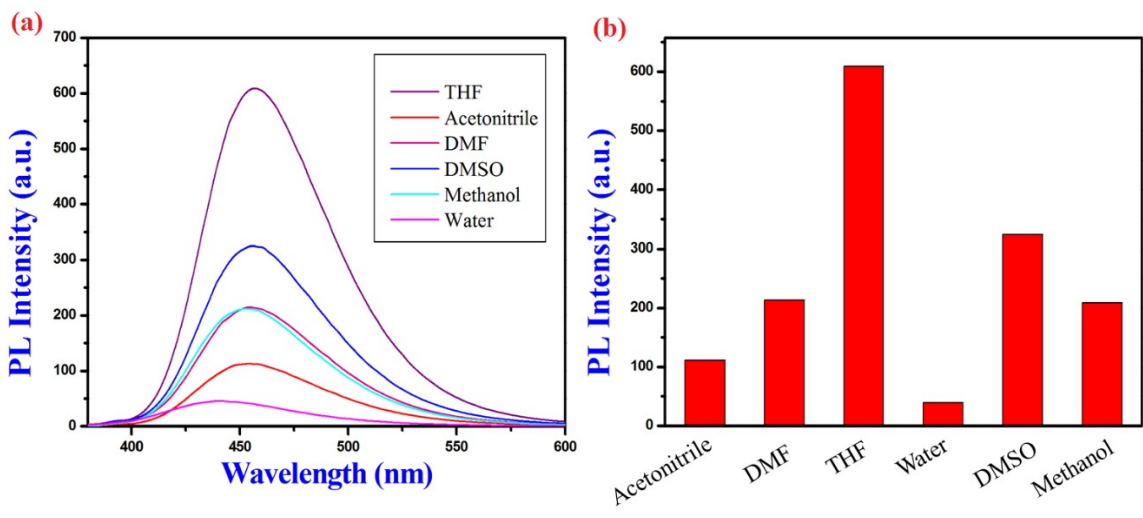
Fig. S11: (a) Fluorescence emission data of PAP with Zn^{2+} in various solvent, (b) graphical presentation of emission intensity of PAP with Zn^{2+} in various solvent at 457nm.
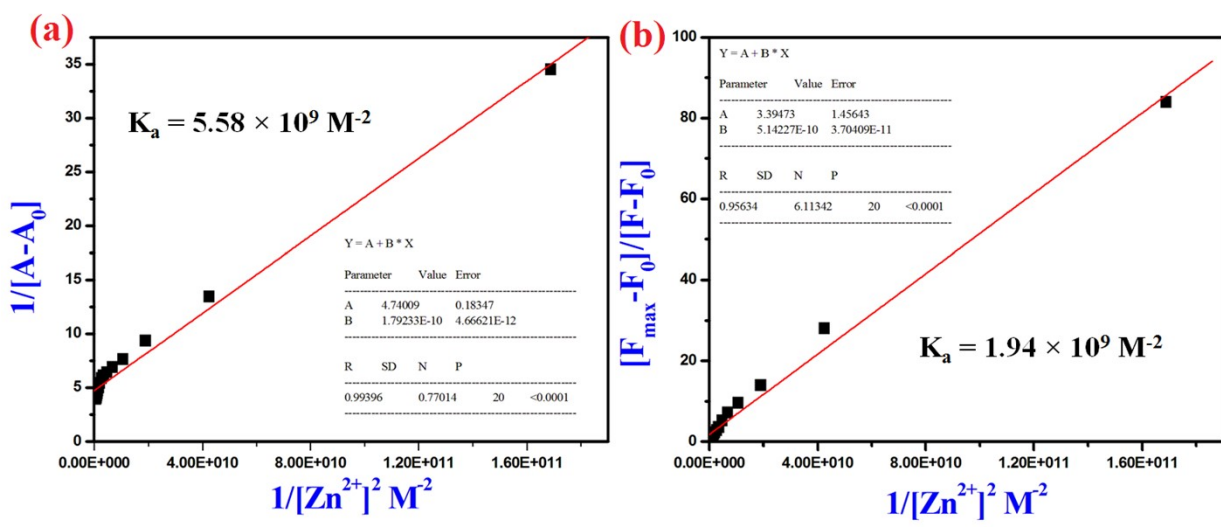
Fig. S12: (a) Binding constant determination plot using Benesi-Hildebrand (B-H) method from absorbance data, (b) Binding constant determination plot using Benesi-Hildebrand (B-H) method from emission intensity data.
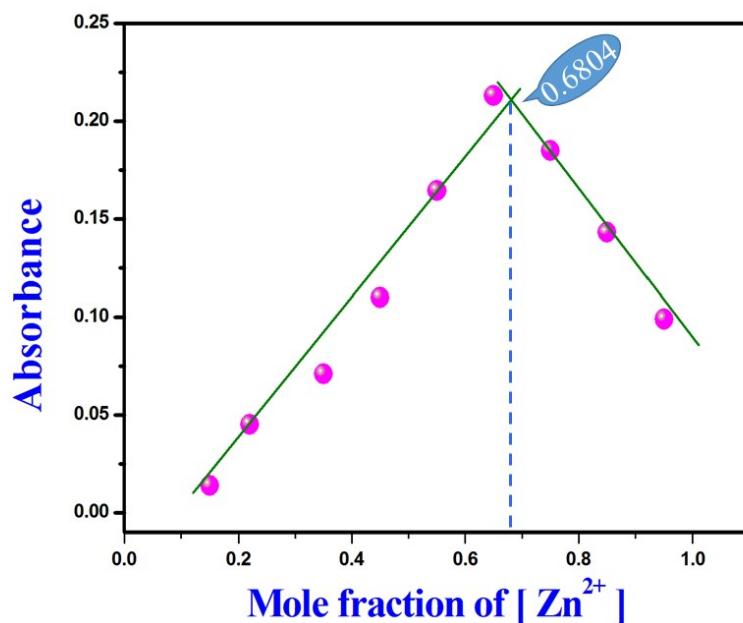
Fig. S13: Job's plot of PAP in presence of Zn^{2+} using continuous variation method, indicating the 1:2 (L : M) stoichiometry at 457 nm.
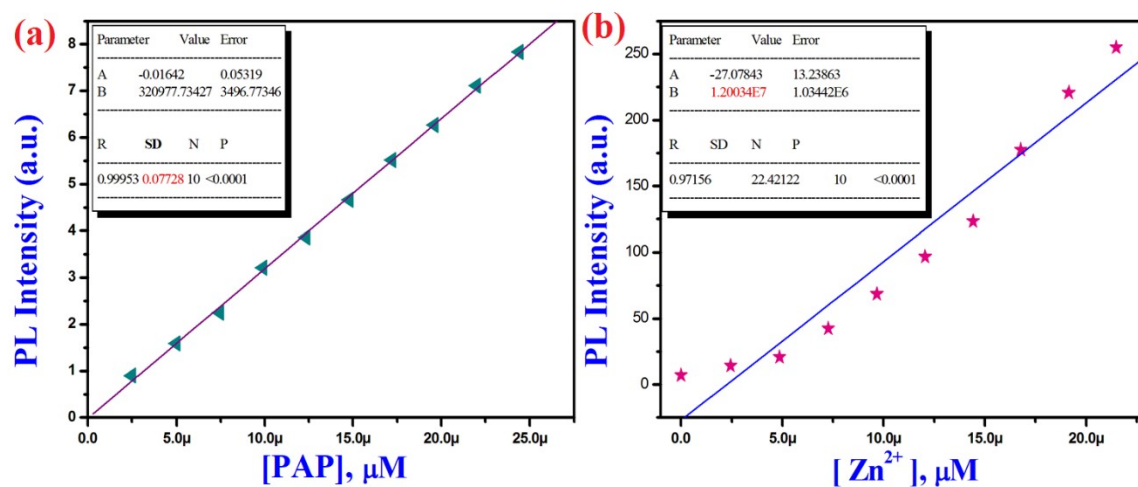
Fig. S14: (a) Plot of fluorescence intensity vs. concentration of PAP for measuring standard deviation of LOD experiment (λ_{ex}: 350 nm, λ_{em}: 440 nm). (b) Plot of fluorescence intensity vs. concentration of Zn^{2+} for measuring slope of LOD experiment (λ_{ex}: 350 nm, λ_{em}: 457 nm) [LOD (Zn^{2+}) = (3 × 0.07728) / (1.2×10^7) M =1.93 × 10^{-8}M. (excitation/emission slit: 5nm).
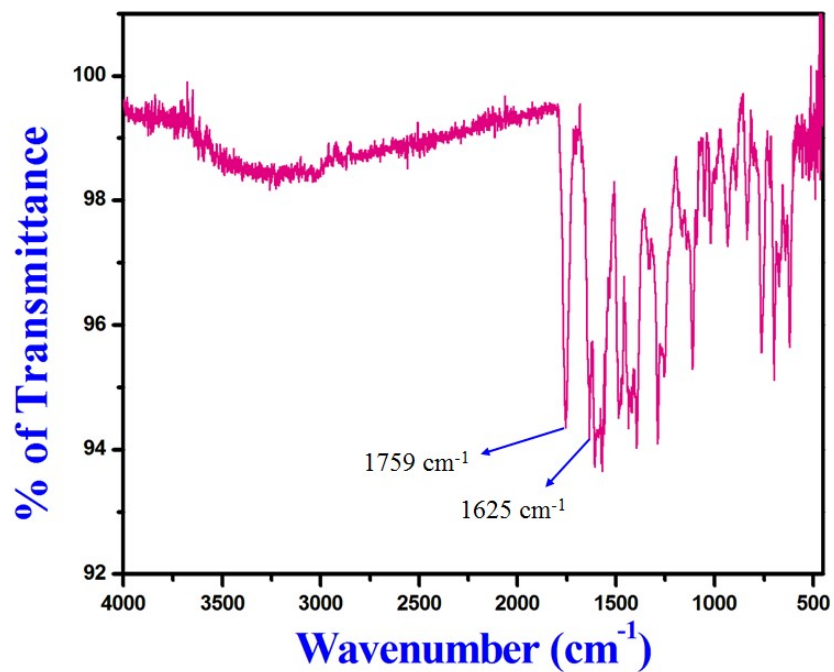
Fig. S15: FT-IR spectra of $[(PAP)Zn_2]^{2+}$.
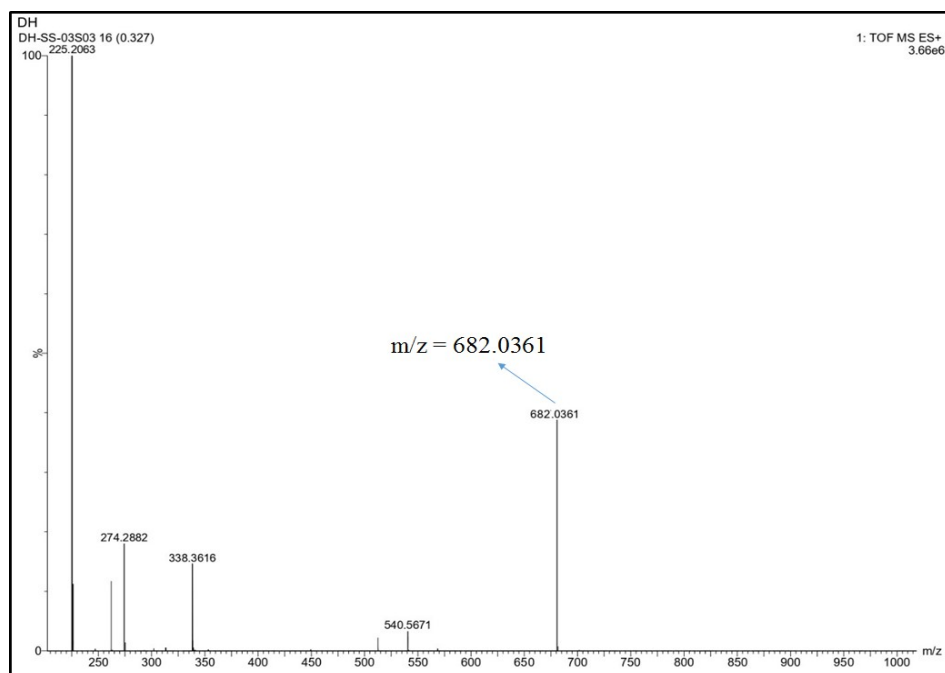
Fig. S16: ESI-MS spectrometric data of $[(PAP)Zn_2]^{2+}$.
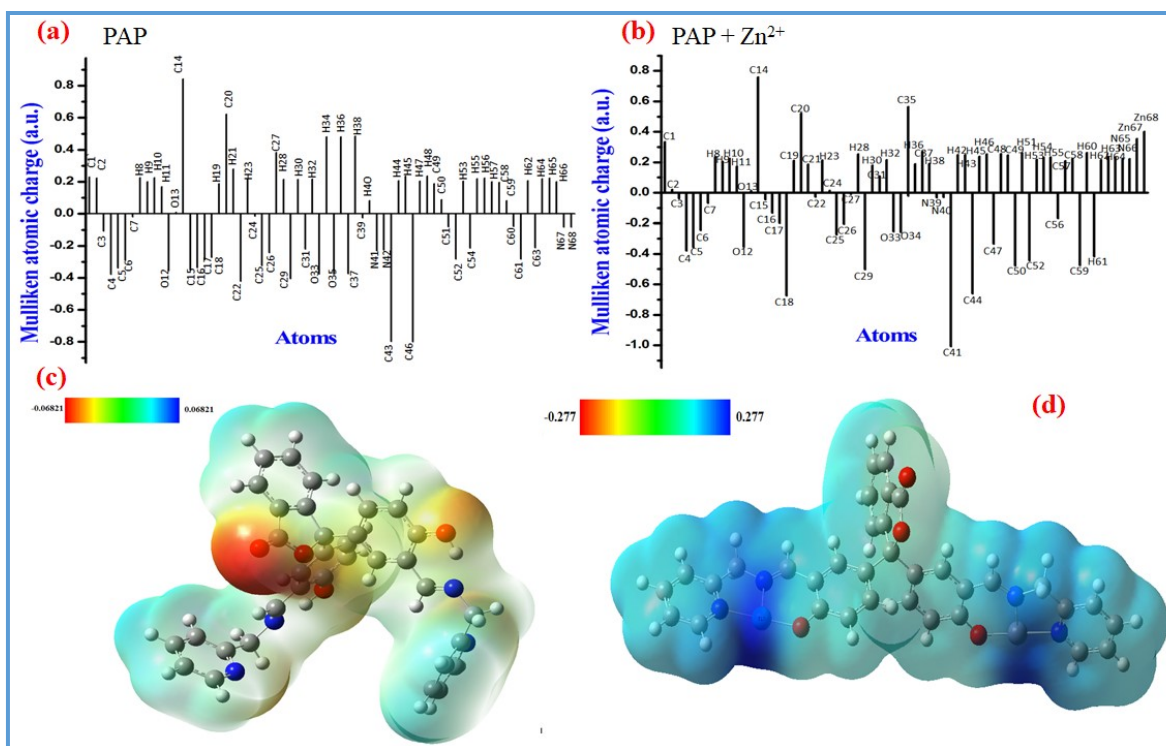
Fig. S17: Mulliken atomic charges obtained at the B3LYP/6-311++G(d,p) level of theory of (a) PAP, (b) PAP-Zn^{2+}, electrostatic potential map of (c) PAP, (d) PAP-Zn^{2+}.
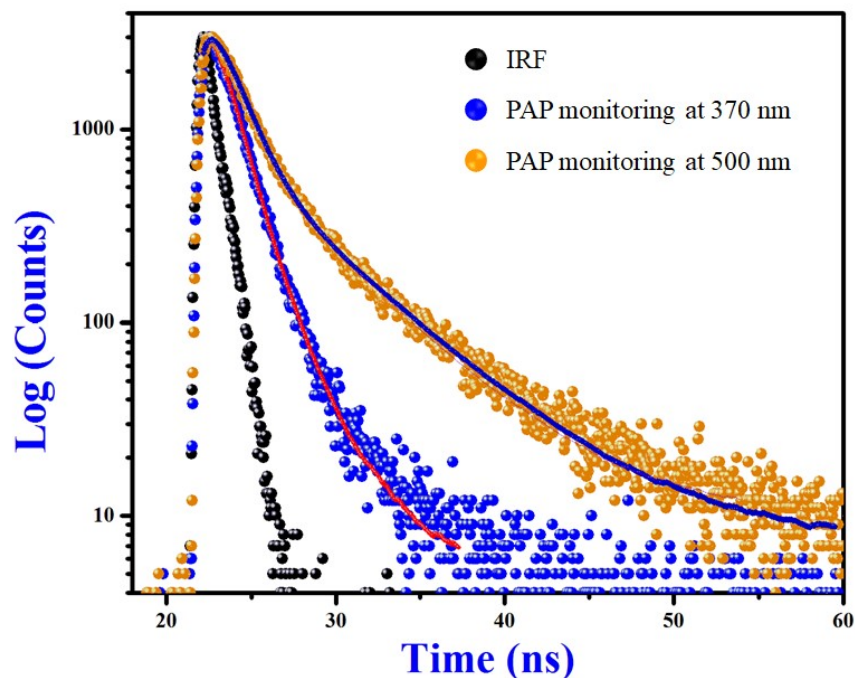
Fig. S18: Fluorescence decay curve of PAP in THF at 360 nm and 500 nm ($\lambda_{ex} \sim 288$ nm).
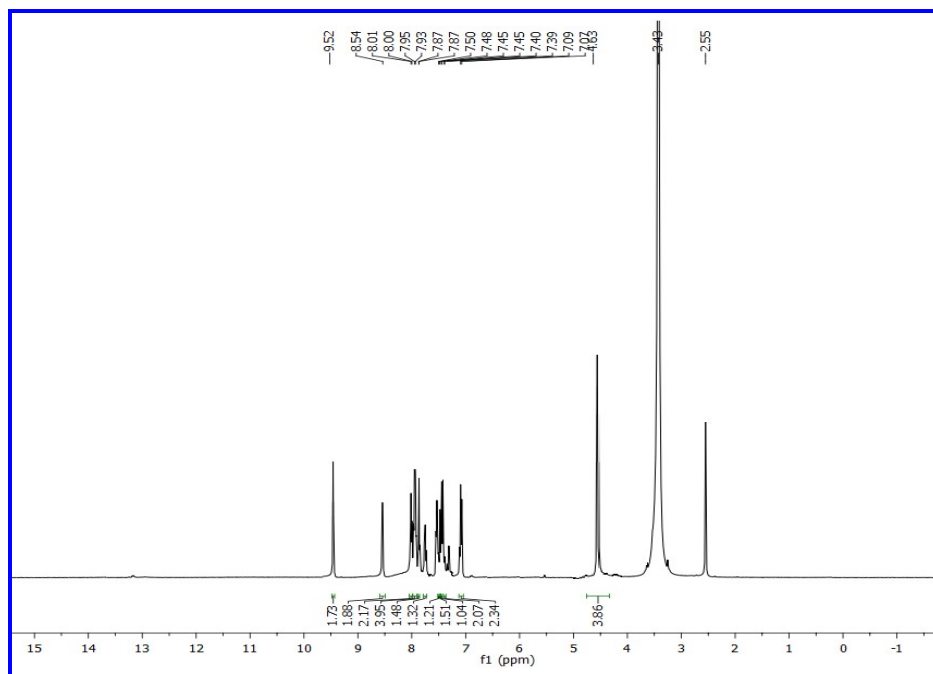
Fig. S19: ^{1}H NMR of PAP-Zn^{2+} complex by mixing 2 equiv. Zn^{2+}with 1 equiv. PAP in DMSO-d$_6$ medium.
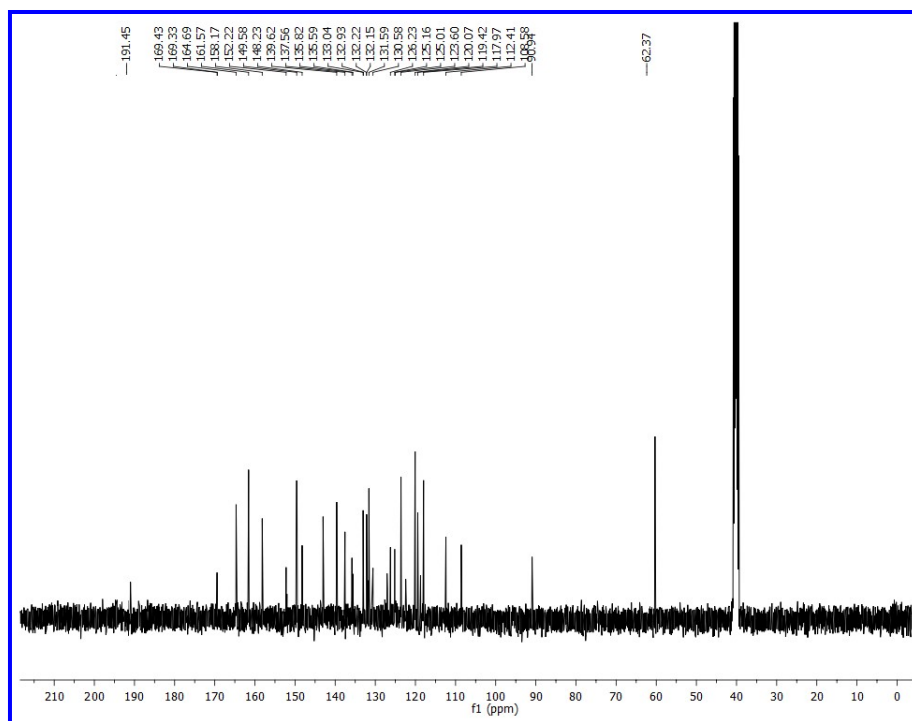
Fig. S20: ^{13}C NMR of PAP-Zn^{2+} complex by taking 2 equiv. Zn^{2+} in DMSO-d$_6$ medium.
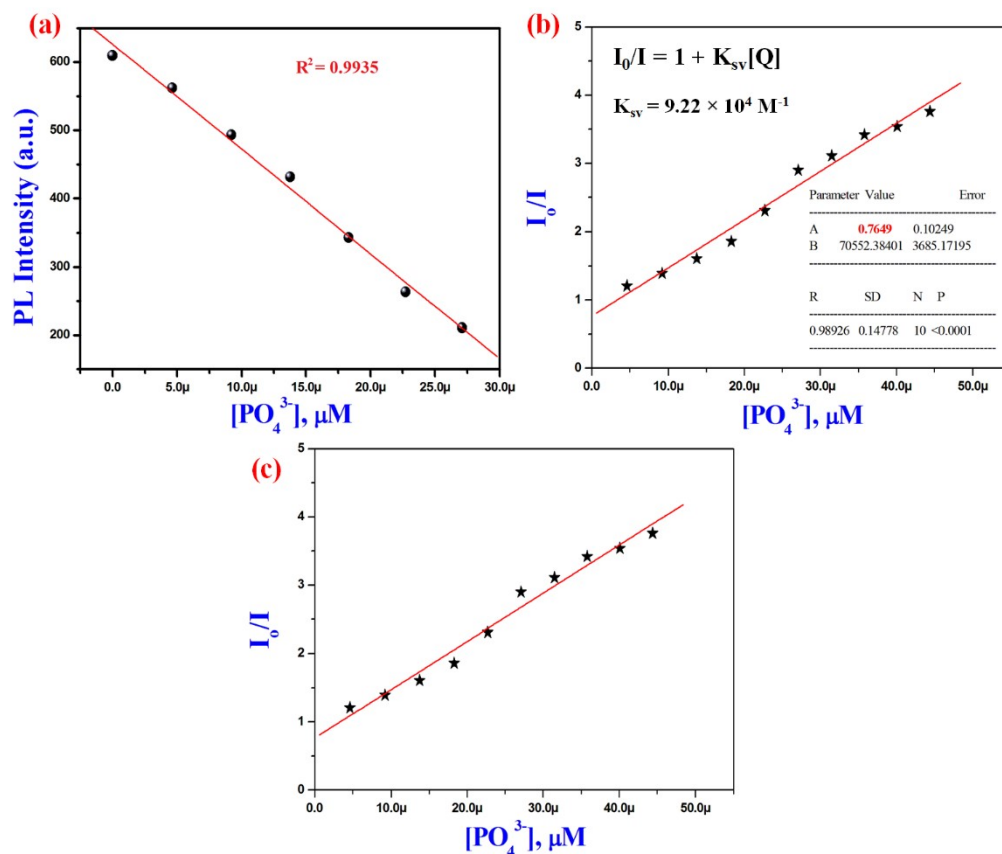
Fig. S21: (a) The linear response of the sensor with PO_4^{3-} from 0 μM to 27 μM; (b) Stern-Volmer (S-V) plot of the fluorescence quenching of PAP-Zn^{2+} complex in THF/water (9.5/0.5, v/v) in response to PO_4^{3-} ions, (c) Fluorescence intensity of PAP-Zn^{2+} complex versus PO_4^{3-} ion concentration plot with error Bars for measuring the detection limit [LOD (PO_4^{3-}) = 8.3 μM].
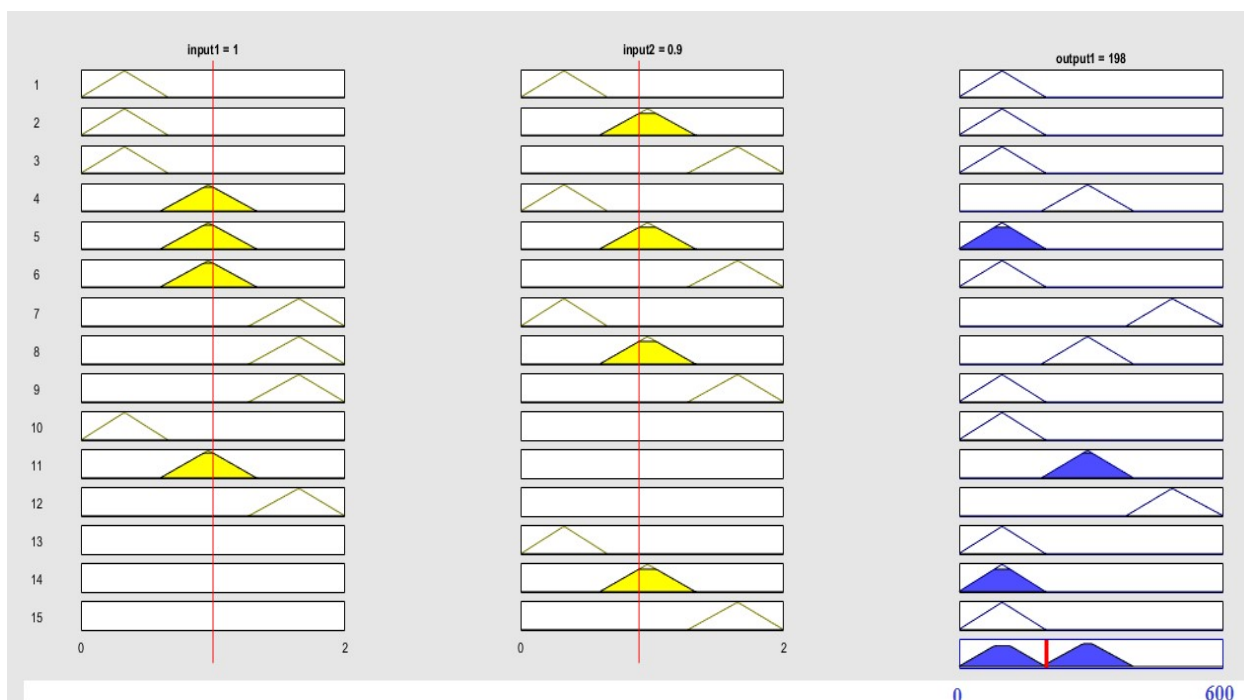
Fig. S22: Mamdani rule view for PAP, PAP-Zn^{2+} and PAP-Zn^{2+}-PO$_4^{3-}$.
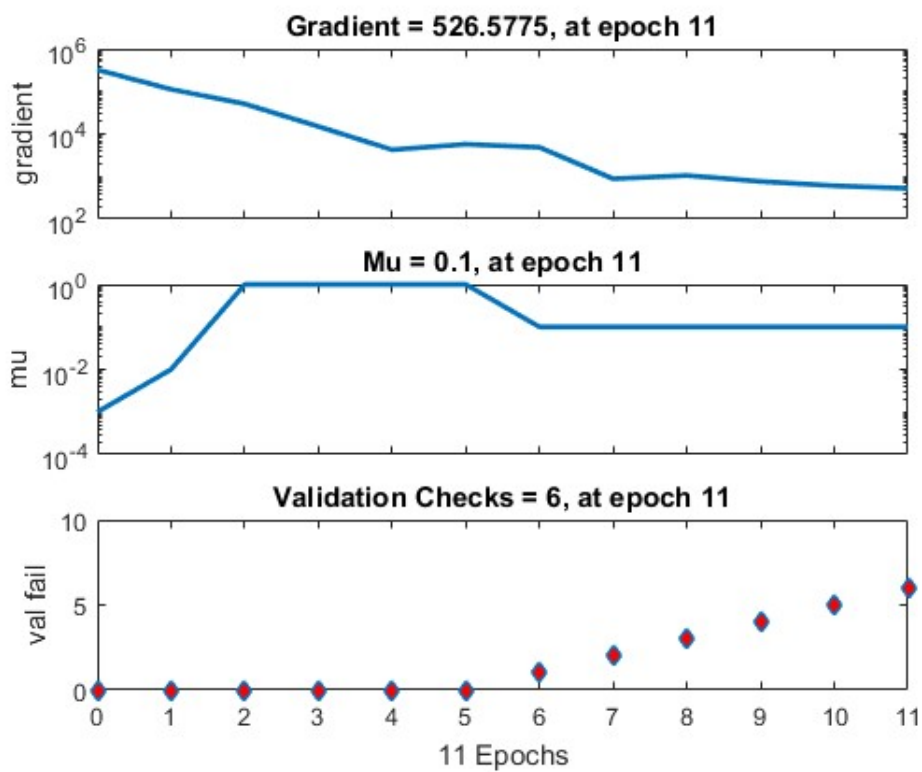
Fig. S23: Training state of the ANN model of PAP, PAP-Zn^{2+} and PAP-Zn^{2+}-PO$_4^{3-}$ (monitoring wavelength at 457nm) up to epoch 11.
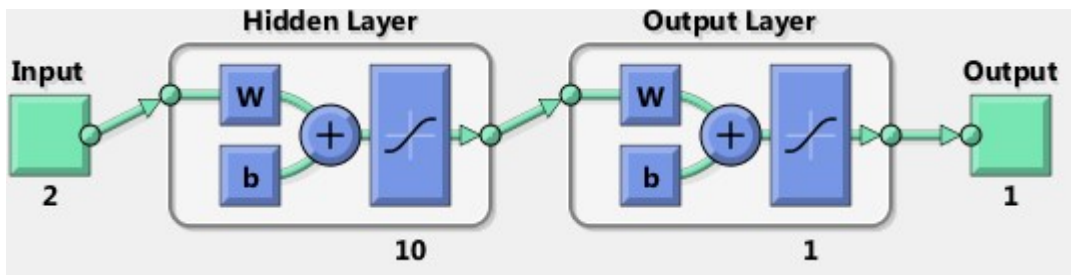
Fig. S24: Artificial neural network model consisting of 2 inputs, 10 hidden layers and 1 output.
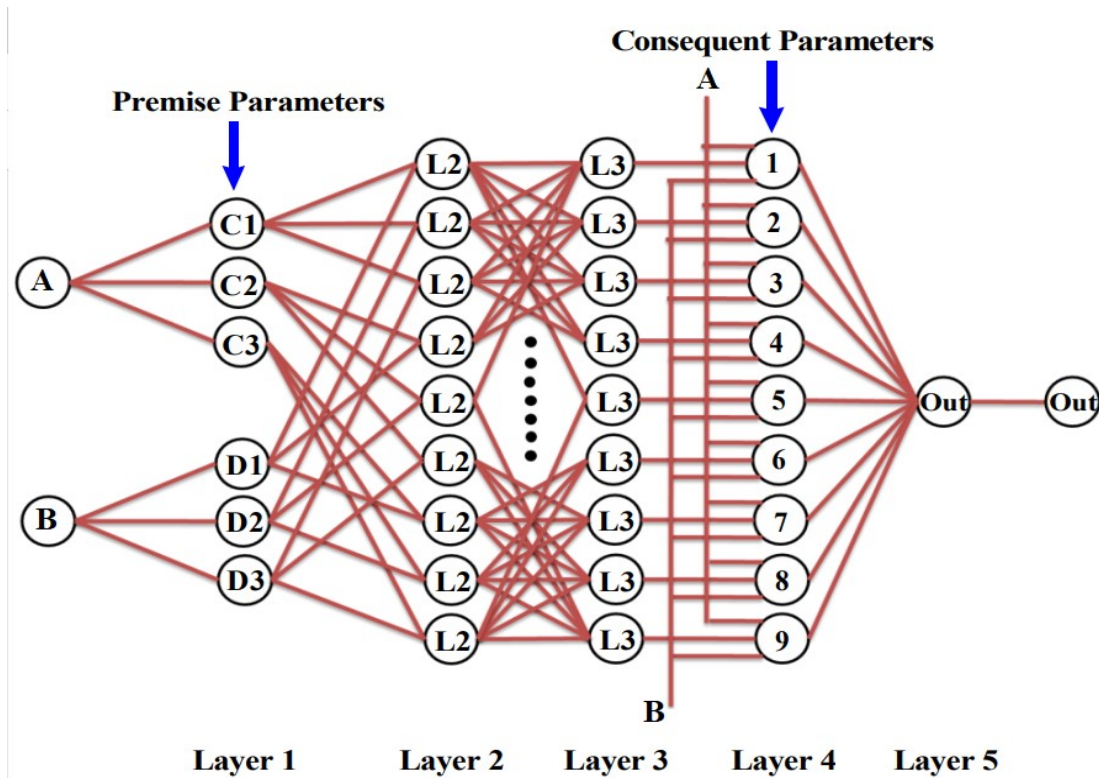
Fig. S25: Schematic sketch of ANFIS network comprising of two inputs, five layers and one output.
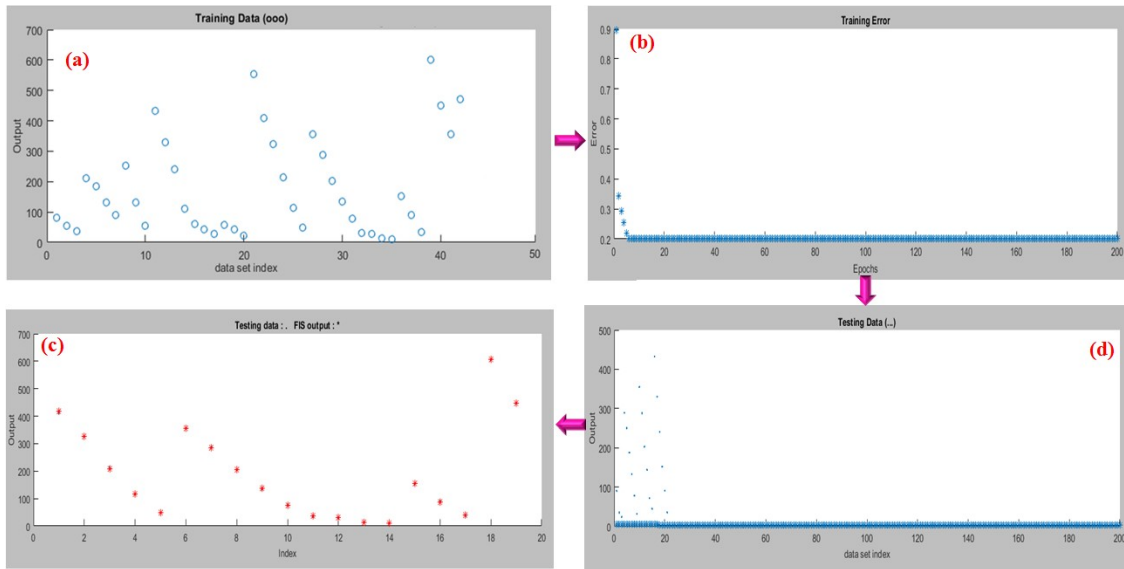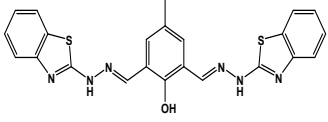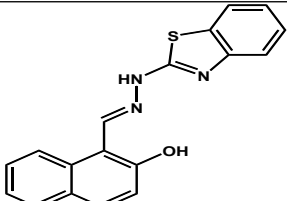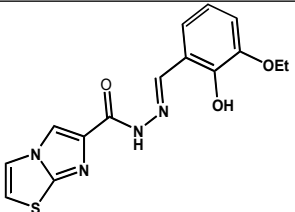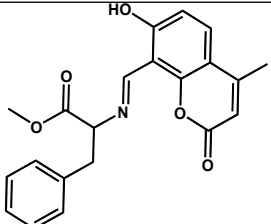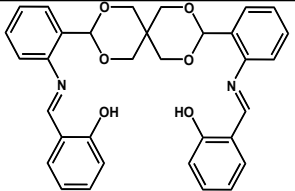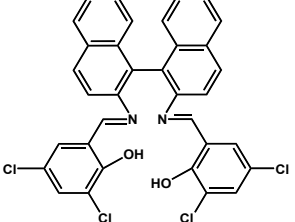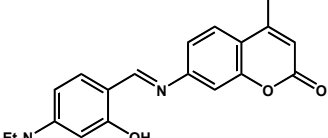
Fig. S26: a) Data set to train the ANFIS network, (b) Root mean square error (RMSE) minimization up to 200 epochs, (c) Data for testing the accuracy of the network output, (d) Combination of testing data and the FIS output.
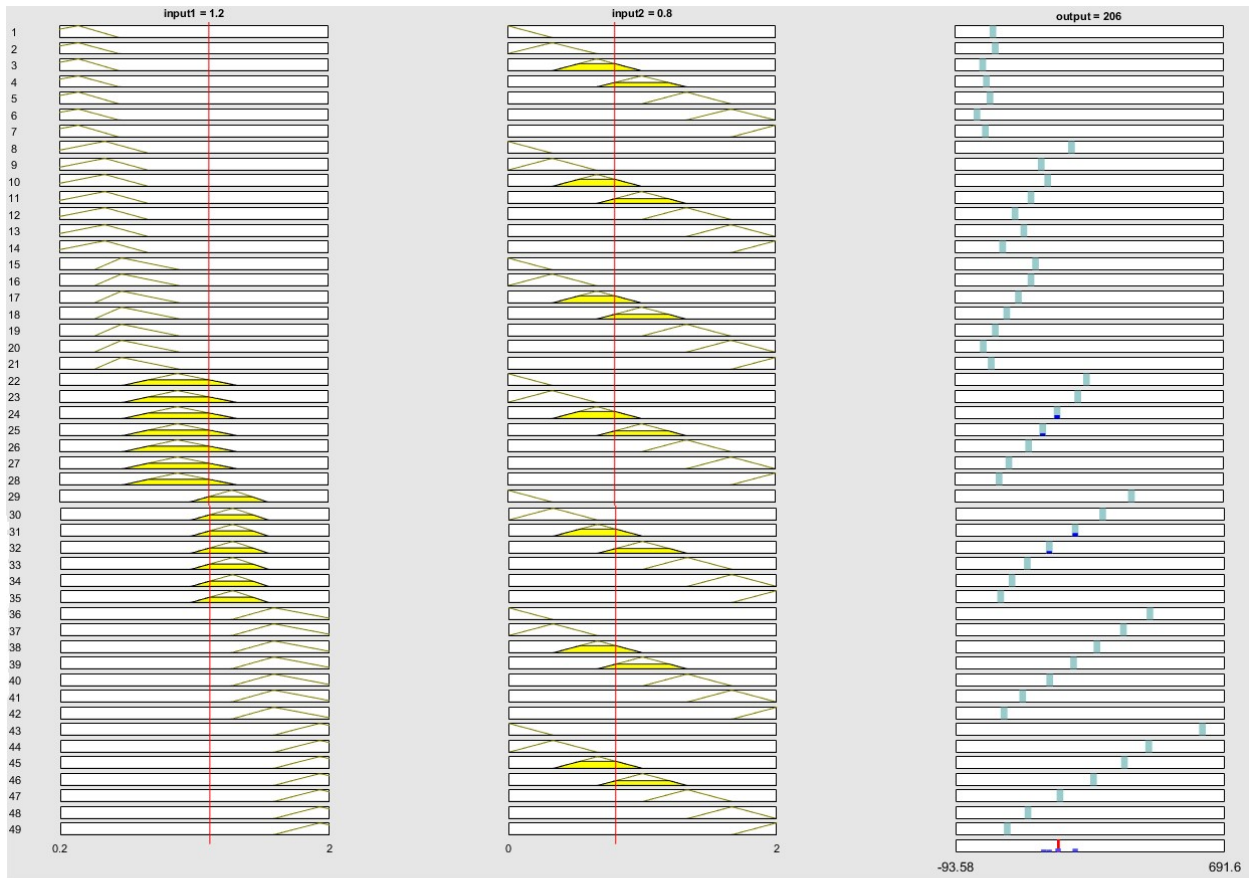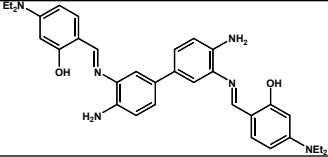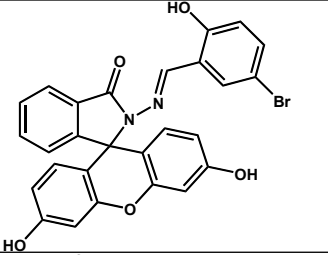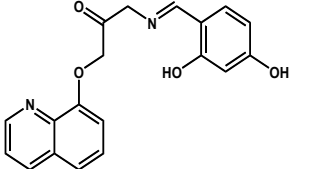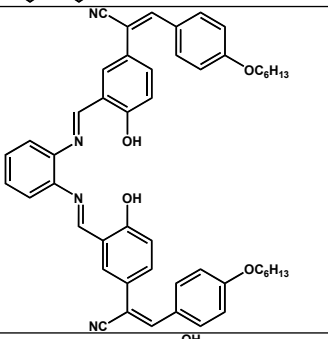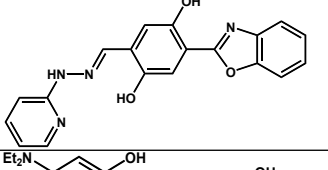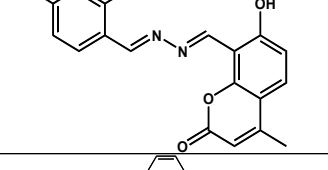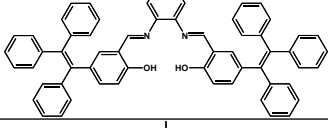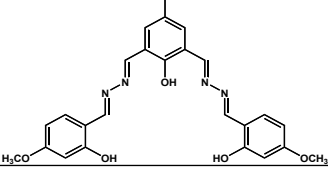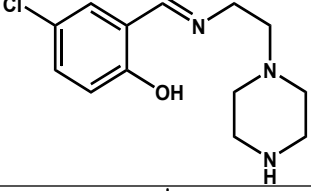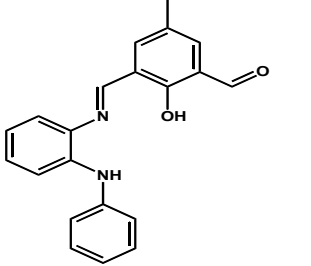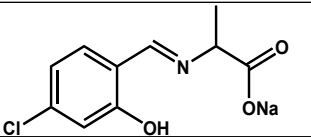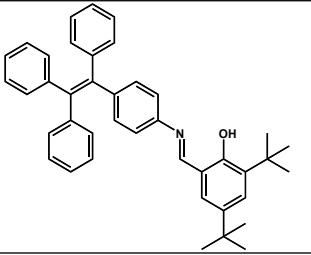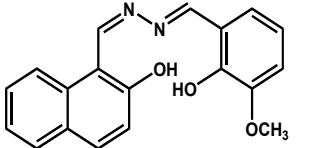
Fig. S27: Sugeno rule view for PAP (monitoring wavelength at 457 nm).

Table S1: Comparative table of fluorescent chemosensors to detect Zn^{2+}.
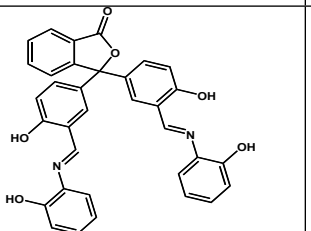
Sl. No.	Probe Molecule	Solvent medium	Analytes	Detection limit (M)	Fuzzy logic operation	Reference
1.		Buffered ethanol (1 : 1 EtOH : 10 mM HEPES, p^H - 7.2)	Zn^{2+}	7.1×10^{-10}	No	[1]
2.		MeOH/aqueous HEPES buffer	Zn^{2+}, Cd^{2+}	6.5×10^{-7}, 2.1×10^{-6}	No	[2]
3.		Ethanol/H_2O buffer Solution (v/v=9:1, tris=10 mM, pH=7.4).	Zn^{2+}	1.2×10^{-9}	No	[3]
4.		ACN/water	Zn^{2+}	3.43×10^{-9}	No	[4]
5.		(EtOH/Tris-HCl, v/v = 4/1, p^H = 7.4)	Zn^{2+}	1.37×10^{-6}	No	[5]
6.		Tetrahydrofuran (THF)	Zn^{2+} (Fluorometric), Cu^{2+} (Colorimetric)	-	No	[6]
7.		DMF-H_2O (v/v, 9:1)	Zn^{2+}	2.59×10^{-6}	No	[7]
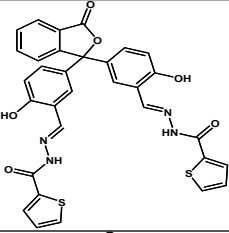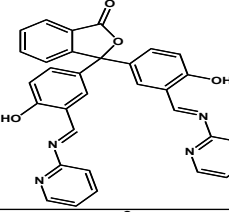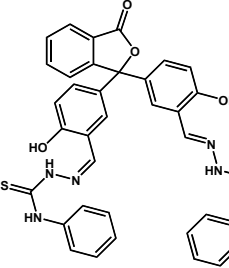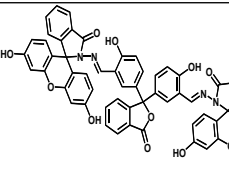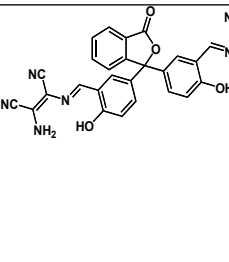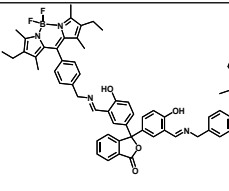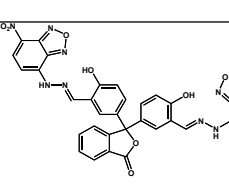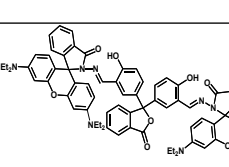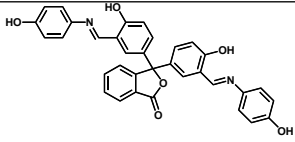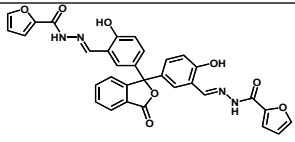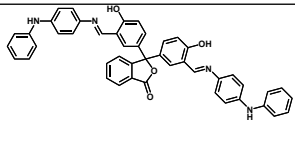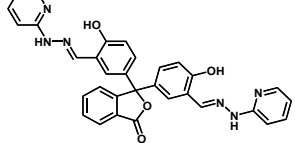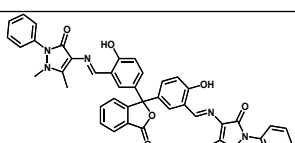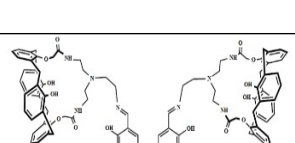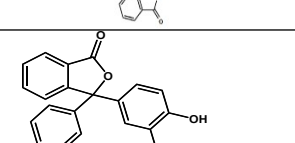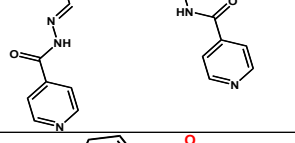
No.	Structure	Solvent	Ion	Detection limit	Sensing	Ref.
8.		Dimethyl formamide (DMF)	Zn^{2+}	8.6×10^{-9}	No	[8]
9.		ethanol-water (9:1,v/v,15 µM HEPES p^H 7.2)	Zn^{2+}	1.59×10^{-6}	No	[9]
10.		Ethanol	Zn^{2+}	3.5×10^{-7}	No	[10]
11.		THF/H_2O (5/95) solutions	Zn^{2+} (fluorometric), Cu^{2+} (Colorimetric)	1.8×10^{-6}, 2.3×10^{-7}	No	[11]
12.		EtOH : HEPES = 1 : 1 (p^H =7.2)	Zn^{2+}	-	No	[12]
13.		Ethanol	Zn^{2+}	3.03×10^{-8}	No	[13]
14.		THF/water mixture (v/v = 1/1)	Zn^{2+}	3.89×10^{-8}	No	[14]
15.		DMSO/water (9 : 1, v/v)	Zn^{2+}, Cd^{2+}, I^-	2.7×10^{-9} 6.6×10^{-9} 5×10^{-9}	No	[15]

Sl. No.	Probe Molecule	Solvent medium	Analytes	Detection limit (M)	Application of Artificial Intelligence	Reference
16.		9:1 methanol water (p^H = 7.4)	Zn^{2+}, Cu^{2+}, F^-	3.21×10^{-8}, 2.13×10^{-8} 3.55×10^{-7}	No	[16]
17.		10 mM HEPES, water/DMSO v/v 3 : 1, p^H 7.4	Zn^{2+}	1.13×10^{-9}	No	[17]
18.		Ethanol	Zn^{2+}	1.55×10^{-6}	No	[18]
19.		DMSO	Zn^{2+}, CO_3^{2-}	8.05×10^{-8}, 7.12×10^{-8}	No	[19]
20.		DMF/H2O (9:1, v/v)	Zn^{2+}	1.1×10^{-7}	No	[20]

Table S2: Reported phenolphthalein based chemosensor article table for the detection of various analytes.

Sl. No.	Probe Molecule	Solvent medium	Analytes	Detection limit (M)	Application of Artificial Intelligence	Reference
21.		HEPES buffer: methanol 1:9; v/v; p^H 7.4	Al^{3+}	1.5×10^{-6}	No	[21]

No.	Structure	Solvent	Ion	Detection limit		Ref.
22.		DMSO	Al^{3+}	1.8×10^{-8}	No	[22]
23.		MeOH-Water	Al^{3+}, Zn^{2+}	1.88×10^{-7} 8.5×10^{-8}	No	[23]
24.		EtOH/H$_2$O (v/v, 80/20, p^H = 7, Britton–Robinson buffer)	CO_3^{2-}	1.47×10^{-8}	No	[24]
25.		EtOH-H2O (v/v, 8/2)	Zn^{2+} Hg^{2+}	5.4×10^{-7} 1.16×10^{-6}	No	[25]
26.		EtOH/H2O (9/1)	Al^{3+} (fluorometric) Cu^{2+} (Colorimetric)	9.2×10^{-8} 2.81×10^{-6}	No	[26]
27.		H$_2$O/acetone (v/v: 1:1)	Sn^{2+}, Al^{3+}	6.31×10^{-8} 6.48×10^{-8}	No	[27]
28.		HEPES aqueous buffer (CH$_3$CN/H$_2$O = 4/1, v/v)	Al^{3+}, Hg^{2+}	1.63×10^{-5}, 1.47×10^{-5}	No	[28]
29.		MeOH-H$_2$O (9:1, v/v, 5 mM HEPES, p^H 7.2)	Al^{3+} Cr^{3+} Cu^{2+} Fe^{3+}	2.27×10^{-6} 1.29×10^{-6} 1.21×10^{-6} 1.75×10^{-6}	No	[29]

No.	Structure	Solvent	Ion	Value	Method	Ref.
30.		C_2H_5OH-HEPES (9/1, v/v, $p^H = 7.0$)	Al^{3+}	1.13×10^{-7}	No	[30]
31.		ACN : HEPES (50:50, v:v, $p^H = 7$)	Al^{3+}	7×10^{-9}	No	[31]
32.		HEPES:CH_3CN (v:v, 1:1, $p^H = 7$)	Cu^{2+}	8.4×10^{-8}	No	[32]
33.		Water	Al^{3+}	2.28×10^{-9}	No	[33]
34.		Ethanol	Al^{3+}	1.5×10^{-8}	No	[34]
35.		CH_3CN/H_2O (8:2, v/v)	Zn^{2+}	1.08×10^{-7}	No	[35]
36.		EtOH:HEPES (9/1;v/v)	Al^{3+} Zn^{2+}	4.4×10^{-9} 4.27×10^{-9}	No	[36]
37.		THF/water (9.5/0.5; v/v)	Zn^{2+}	19.3 nM	Fuzzy, ANN, ANFIS	This work

Table S3: Selective optimized bond lengths and bond angles of complex $[(PAP)Zn_2]^{2+}$.

Bond length (Å)		Bond angle (^{0})	
O1-Zn1 ≈ O2-Zn2	1.90	O1-Zn1-N1 ≈ O2-Zn2-O3	97.23
N1-Zn1 ≈ N3-Zn2	2.01	O1-Zn1-N2 ≈ O2-Zn2-N4	178.83
N2-Zn1 ≈ N4-Zn2	2.02	N1-Zn1-N2 ≈ N3-Zn2-N4	83.06

Table S4: Frontier molecular orbitals of PAP and Zn^{2+}-PAP complex calculated by the B3LYP/6-311++G(d,p) method.

Structures	I	A	E_g	μ	χ	Ŋ	ζ	ω
PAP	6.368	1.92	4.45	-4.14	4.14	2.22	0.224	3.85
PAP+Zn^{2+}	8.84	2.865	3.87	-4.8	4.8	1.93	0.258	5.95

*I = ionization potential, A = Electron affinity, E_g = HOMO-LUMO energy gap, μ = Chemical potential, χ = Electronegativity, Ŋ = Chemical hardness, ζ = Global softness and ω = electrophilicity index.

Table S5: Experimental and computed value of absorption wavelength (nm) of PAP and $[(PAP)Zn_2]^{2+}$.

Ligand & Complex	Experimental (nm)	Theoretical (nm)	Composition	Energy (eV)	*f*
PAP	323	321	HOMO → LUMO	3.86	0.0039
	289	287	HOMO-1 → LUMO+2	4.31	0.0253
	260	259	HOMO-1 → LUMO+4	4.77	0.0019
PAP + Zn^{2+}	373	365	HOMO → LUMO	3.38	0.2036
	262	264	HOMO-3 → LUMO+1	4.69	0.0852

Table S6: Selected Unscaled Vibrational Frequencies of Probe PAP and its Zn complex.

Structures		Experimental (cm^{-1})	Theoretical (cm^{-1})
PAP	O-H	3382	3290
	C-H	2880	2913
	-COO-	1759	1782
	C=N	1633	1650
PAP + Zn^{2+}	C-H	-	3016
	-COO-	1759	1785
	C=N	1625	1632

Table S7: Rules for the fuzzy logic system by taking Zn^{2+} (input 1) and PO_4^{3-} (input 2) as the inputs and emission intensity at 457 nm as the outputs for PAP. The rules comprise of the following statements

1. If (input1 is Low) and (input2 is Low) then (output1 is Low) (1)
2. If (input1 is Low) and (input2 is Medium) then (output1 is Low) (1)
3. If (input1 is Low) and (input2 is High) then (output1 is Low) (1)
4. If (input1 is Medium) and (input2 is Low) then (output1 is Medium) (1)
5. If (input1 is Medium) and (input2 is Medium) then (output1 is Low) (1)
6. If (input1 is Medium) and (input2 is High) then (output1 is Low) (1)
7. If (input1 is High) and (input2 is Low) then (output1 is High) (1)
8. If (input1 is High) and (input2 is Medium) then (output1 is Low) (1)
9. If (input1 is High) and (input2 is High) then (output1 is Low) (1)
10. If (input1 is Low) then (output1 is Low) (1)
11. If (input1 is Medium) then (output1 is Medium) (1)
12. If (input1 is High) then (output1 is High) (1)
13. If (input2 is Low) then (output1 is Low) (1)
14. If (input2 is Medium) then (output1 is Low) (1)
15. If (input2 is High) then (output1 is Low) (1)

Table S8: Different values of emission intensity as a function of $n_{Zn^{2+}}/n_1$ and $n_{PO4^{3-}}/n_1$ for PAP.

No. of obs.	Equiv. of Zn^{2+}	Equiv. of PO_4^{3-}	Emission intensity at 457nm
1	0.2	0	80
2	0.2	0.4	56
3	0.2	0.8	36
4	0.8	0	212
5	0.8	0.4	185
6	0.8	0.8	132
7	2	1.2	252
8	2	1.6	131
9	2	2	55
10	1.4	0	432
11	1.4	0.4	330
12	1.4	0.8	240
13	0.6	0.8	112
14	0.6	1.2	62
15	0.6	1.6	42
16	0.6	2	28
17	0.4	1.2	58
18	0.4	1.6	42
19	0.4	2	21
20	1.8	0	555
21	1.8	0.4	410
22	1.8	0.8	324
23	1.6	1.2	215
24	1.6	1.6	115
25	1.6	2	48
26	1.2	0	355
27	1.2	0.4	288
28	1.2	0.8	203
29	1	1.2	133
30	1	1.6	78
31	1	2	32
32	0.2	1.2	28

33	0.2	1.6	12
34	0.2	2	10
35	1.4	1.2	152
36	1.4	1.6	91
37	1.4	2	35
38	2	0	602
39	2	0.4	450
40	2	0.8	355
41	1.6	0	470
42	1.6	0.4	384
43	1.6	0.8	292
44	1.8	1.2	216
45	1.8	1.6	132
46	1.8	2	54
47	0.4	0	132
48	0.4	0.4	91
49	0.4	0.8	77
50	0.8	1.2	90
51	0.8	1.6	35
52	0.8	2	24
53	1.2	1.2	144
54	1.2	1.6	72
55	1.2	2	45
56	0.6	0	188
57	0.6	0.4	139
58	1	0	289
59	1	0.4	250
60	1	0.8	188

Table S9: Rules for the ANFIS (based on Sugeno's method) by taking Zn^{2+} as input 1 and PO_4^{3-} as input 2, whereas emission intensity at 457 nm as the output. The rules comprise of the following statements.

1. If (input1 is in1mf1) and (input2 is in2mf1) then (output is out1mf1) (1)
2. If (input1 is in1mf1) and (input2 is in2mf2) then (output is out1mf2) (1)
3. If (input1 is in1mf1) and (input2 is in2mf3) then (output is out1mf3) (1)
4. If (input1 is in1mf1) and (input2 is in2mf4) then (output is out1mf4) (1)
5. If (input1 is in1mf1) and (input2 is in2mf5) then (output is out1mf5) (1)
6. If (input1 is in1mf1) and (input2 is in2mf6) then (output is out1mf6) (1)
7. If (input1 is in1mf1) and (input2 is in2mf7) then (output is out1mf7) (1)
8. If (input1 is in1mf2) and (input2 is in2mf1) then (output is out1mf8) (1)
9. If (input1 is in1mf2) and (input2 is in2mf2) then (output is out1mf9) (1)
10. If (input1 is in1mf2) and (input2 is in2mf3) then (output is out1mf10) (1)
11. If (input1 is in1mf2) and (input2 is in2mf4) then (output is out1mf11) (1)
12. If (input1 is in1mf2) and (input2 is in2mf5) then (output is out1mf12) (1)
13. If (input1 is in1mf2) and (input2 is in2mf6) then (output is out1mf13) (1)
14. If (input1 is in1mf2) and (input2 is in2mf7) then (output is out1mf14) (1)
15. If (input1 is in1mf3) and (input2 is in2mf1) then (output is out1mf15) (1)
16. If (input1 is in1mf3) and (input2 is in2mf2) then (output is out1mf16) (1)
17. If (input1 is in1mf3) and (input2 is in2mf3) then (output is out1mf17) (1)
18. If (input1 is in1mf3) and (input2 is in2mf4) then (output is out1mf18) (1)
19. If (input1 is in1mf3) and (input2 is in2mf5) then (output is out1mf19) (1)
20. If (input1 is in1mf3) and (input2 is in2mf6) then (output is out1mf20) (1)
21. If (input1 is in1mf3) and (input2 is in2mf7) then (output is out1mf21) (1)
22. If (input1 is in1mf4) and (input2 is in2mf1) then (output is out1mf22) (1)
23. If (input1 is in1mf4) and (input2 is in2mf2) then (output is out1mf23) (1)
24. If (input1 is in1mf4) and (input2 is in2mf3) then (output is out1mf24) (1)
25. If (input1 is in1mf4) and (input2 is in2mf4) then (output is out1mf25) (1)
26. If (input1 is in1mf4) and (input2 is in2mf5) then (output is out1mf26) (1)
27. If (input1 is in1mf4) and (input2 is in2mf6) then (output is out1mf27) (1)
28. If (input1 is in1mf4) and (input2 is in2mf7) then (output is out1mf28) (1)
29. If (input1 is in1mf5) and (input2 is in2mf1) then (output is out1mf29) (1)
30. If (input1 is in1mf5) and (input2 is in2mf2) then (output is out1mf30) (1)
31. If (input1 is in1mf5) and (input2 is in2mf3) then (output is out1mf31) (1)
32. If (input1 is in1mf5) and (input2 is in2mf4) then (output is out1mf32) (1)
33. If (input1 is in1mf5) and (input2 is in2mf5) then (output is out1mf33) (1)
34. If (input1 is in1mf5) and (input2 is in2mf6) then (output is out1mf34) (1)
35. If (input1 is in1mf5) and (input2 is in2mf7) then (output is out1mf35) (1)
36. If (input1 is in1mf6) and (input2 is in2mf1) then (output is out1mf36) (1)
37. If (input1 is in1mf6) and (input2 is in2mf2) then (output is out1mf37) (1)
38. If (input1 is in1mf6) and (input2 is in2mf3) then (output is out1mf38) (1)
39. If (input1 is in1mf6) and (input2 is in2mf4) then (output is out1mf39) (1)
40. If (input1 is in1mf6) and (input2 is in2mf5) then (output is out1mf40) (1)
41. If (input1 is in1mf6) and (input2 is in2mf6) then (output is out1mf41) (1)
42. If (input1 is in1mf6) and (input2 is in2mf7) then (output is out1mf42) (1)
43. If (input1 is in1mf7) and (input2 is in2mf1) then (output is out1mf43) (1)
44. If (input1 is in1mf7) and (input2 is in2mf2) then (output is out1mf44) (1)
45. If (input1 is in1mf7) and (input2 is in2mf3) then (output is out1mf45) (1)
46. If (input1 is in1mf7) and (input2 is in2mf4) then (output is out1mf46) (1)
47. If (input1 is in1mf7) and (input2 is in2mf5) then (output is out1mf47) (1)
48. If (input1 is in1mf7) and (input2 is in2mf6) then (output is out1mf48) (1)
49. If (input1 is in1mf7) and (input2 is in2mf7) then (output is out1mf49) (1)

EXPERIMENTAL SECTION

Physical Measurements:

^{1}H NMR spectra was recorded on a Bruker ASCEND spectrometer operating at 400 MHz in CDCl$_3$ & DMSO-d$_6$. The ESI-MS was recorded on Qtof Micro YA263 mass spectrometer. UV-vis spectroscopic measurements were carried out in a 1 cm quartz cuvette with a Shimadzu UV-1800 spectrophotometer. Fluorescence spectra were recorded using Hitachi F-7100 Fluorescence Spectrophotometer. Fluorescence lifetimes were determined from time-resolved intensity decay by the method of time correlated single-photon counting (TCSPC) measurements using a picoseconds diode laser (IBH) and the signals are collected at magic angles (54.7°). The instrument response function of the instrument is ~90 ps. The fluorescence decay data were collected on a Hamamatsu MCPPMT (R3809) and were analyzed by using IBH DAS 6.3 software. Nano LED at 372 nm was used as the excitation source. The Fourier transform infrared (FT-IR) spectra were obtained in the range of 4000-400 cm^{-1} on a Perkin Elmer Spectrum-Two FTIR spectrometer. Ground-state geometry of PAP and Zn^{2+}-PAP complex were optimized using the density functional theory (DFT) with B3LYP hybrid functional at the basis set level of 6-311++G(d, p). All the theoretical calculations were performed using Gaussian 16 package program. Dissociation constant has been found out from non-linear fittings by suitable computer-fit equation. LOD is calculated by linear fitting curve. All Fuzzy, ANN and ANFIS work done by MATLAB 2017a software.

Sample Preparation for UV-Vis and Fluorescence Spectroscopic Studies:

A stock solution of PAP (1.0 mM) was prepared in THF. Stock solutions of various metal ions (1.0 mM, Na$^+$, Ca^{2+}, Cu^{2+}, Ba^{2+}, Zn^{2+}, Mg^{2+}, Cd^{2+}, Hg^{2+}, Fe^{3+}, Al^{3+}, Pb^{2+}, Cr^{3+}, Co^{2+} and Ni^{2+}(as their acetate or nitrate salts)) are prepared in deionized water. Stock solution of various anionic solutions (HAsO$_4^-$, AsO$_2^-$, SO$_4^{2-}$, HSO$_3^-$, HSO$_4^-$, NO$_3^-$, H$_2$PO$_4^-$, HPO$_4^{2-}$, AcO$^-$, F$^-$, Cl$^-$, Br$^-$, I$^-$, S$_2$O$_4^{2-}$, CN$^-$, SCN$^-$, PO$_4^{3-}$, and S$_2$O$_3^{2-}$ (Na salts)) are also made in deionized water. In titration experiments, a quartz optical cell of 1 cm path length was filled with a 2.0 mL solution of PAP to which the stock solutions of metal ions were gradually added using a micro-pipette. In selectivity experiments, the test samples were prepared by placing appropriate amounts of the cations stock into 2.0 mL of PAP solution (25μM). All UV-vis. and fluorescence titration experiments were carried out in THF-water (9.5:0.5, v/v) medium. For fluorescence measurements, excitation was

provided at 350 nm, and emission was acquired from 365 nm to650 nm (excitation/emission spectral band width is 5nm).

Determination of Fluorescence Quantum Yield:

The fluorescence quantum yield (φ) was calculated using the following equation;

$$\Phi sample = \frac{OD\text{standard} \times A\text{sample}}{A\text{standard} \times OD\text{sample}} \times \Phi standard$$

Where A represents the area under the fluorescence spectral curve and OD symbolizes the optical density of the compound at the excitation wavelength. Quinine sulfate ($\Phi_r = 0.546$ in $1NH_2SO_4$) was used as a reference compound to measure the fluorescence quantum yield.

Detection Limit:

The detection limit was calculated on the basis of the fluorescence titration. The fluorescence emission spectrum of PAP as a function of its increasing concentration was measured five times, and the standard deviation of blank measurement was calculated. To obtain the slope, the fluorescence emission intensity at 457 nm was plotted against the concentration ofZn^{2+}. The detection limit was calculated using the following equation.

$$\text{Detection limit} = 3\sigma/k$$

Where σ is the standard deviation of blank measurement, and k is the slope of the calibration curve obtained from linear dynamic plot of fluorescence intensity vs. $[Zn^{2+}]$.

Evaluation of binding constant:

Solution of receptor PAP(25 µM) in THF-water (9.5:0.5, v/v) medium was used for both absorbance and emission titration studies for the metal ion,Zn^{2+}.The binding constant K_a of the metal-receptor complex was determined using the Benesi-Hildebrand (B-H) equation separately from absorption as well as emission titration data.

$$\frac{1}{A - A_0} = \frac{1}{A_I - A_0} + \frac{1}{K_a(A_I - A_0)[M^{n+}]m}$$

Where, A_0, A and A_I are the observed absorbance intensity at that particular wavelength in the absence, presence of intermediate concentration of the metal ion $[M^{n+}]$ and with excess metal ion concentrations, respectively.

$$\frac{1}{F - F_0} = \frac{1}{F_{max} - F} + \frac{1}{K_a(F_{max} - F_0)[M^{n+}]m}$$

Where, F_0, F and F_{max} are the observed emission intensity at that particular wavelength in the absence, presence of intermediate concentration of the metal ion $[M^{n+}]$ and with excess metal ion concentrations, respectively.

Fluorescence lifetime measurements:

Fluorescence lifetimes were determined from time-resolved intensity decay by the method of time correlated single-photon counting (TCSPC) measurements using a picoseconds diode laser (IBH) and the signals are collected at magic angles (54.7°). The instrument response function of the instrument is ~90 ps. The fluorescence decay data were collected on a Hamamatsu MCPPMT (R3809) and were analyzed by using IBH DAS 6.3 software. Nano LED at 372 nm was used as the excitation source. The acceptability of the fits was judged by χ^2 criteria and visual inspection of the residuals of the fitted function to the data. Mean (average) fluorescence lifetimes were calculated using the following equation in which α_i is the pre-exponential factor corresponding to the i'th decay time constant, τ_i.

$$\tau_{av} = \frac{\sum \alpha_i \tau_i^2}{\sum \alpha_i \tau_i}$$

A more fine analysis of the data has been undertaken to mark out the contributions from radiative (k_r) and non-radiative (k_{nr}) decay rate constants according to the following equations:

$$k_r = \frac{\varphi_f}{\tau_{av}} \qquad\qquad k_r + k_{nr} = \frac{1}{\tau_{av}}$$

Artificial neural networks (ANNs)

An artificial neural network is a network stimulated by the central nervous system of the animals, primarily the brain. ANNs are often employed to guess functions which could rely on huge number of unknown inputs. Among the two principal categories of neural networks, viz. recurrent (RNN) and feed-forward (FFN), we employed FNN in the present study due to static nature of our system. FNN is the simplest and convenient category of network where the information passes into a particular direction, proceeds, from the input nodes, via the hidden

notes, and finally to the output nodes. Additionally, due to its high efficiency in forecasting static system, we implemented advanced feed-forward back propagation network, namely, ANN-function fitting (ANN-FF) network for deeper understanding and forecasting of the system. Artificial neural network model consisting of 2 inputs, 10 hidden layers and 1 output. In ANN-FF, the relation between the input and output is assumed to be a function, which is approximated using the experimental data. The network diagram of the ANN-FF for the system can be found in Fig. S24, ESI†. It can fit multidimensional mapping problems arbitrarily well when consistent data and enough neurons are designed in the hidden layer. For function fitting of the problem, a neural network is needed to map between a data set of numeric inputs and a set of numeric targets. Hence, each pattern is assigned a number (e.g., 1, 2, 3, 4, etc.)

In this study, a neural network for function fitting was coded in MATLAB 2017a. The input data present the network, while the target data define the desired network output. Table S8 represents the emission intensity outputs upon the action of 60 different combinations of two inputs (input 1=Zn^{2+} and input 2= PO_4^{3-}). Thus, the 60×2 matrix represents the static input data of 60 samples involving 2 inputs, while 60×1 matrix represents the static output data (at 457 nm) of one element. Now, the 60 samples are divided into 3 sets of data. 70% of the data are conferred for the training and the network is corrected according to its error. Now the learning algorithm and the number of neurons in the hidden layer were optimized. 15% data are employed to compute the network generalization and to halt training. When generalization stops improving, the data validation takes place. The remaining 15% data give an independent estimate of the network performance during and after the training, called testing data (Fig. 13a).

Adaptive neuro-fuzzy inference system (ANFIS)

The network framework of the ANFIS is illustrated in Fig. S25, ESI†. It consists of five connected layers (excluding input layer) which is common for the two input dimensions, A and B, both of which possess three fuzzy sets, viz. C1C2C3 for A, while D1D2D3 for B input. We have chosen A number of inputs and B number of fuzzy set to represent each input which in turn implies A×B number of nodes in Layer 1. In Layer 2, all the nodes are interconnected with the membership function output of each input node, yielding a total of B^A node in Layer 2. Layer 3 and 4possess the same number of nodes as that of Layer 2. Layer 5, on the other hand, possess only one node representing the output of the network. Upon considering each input as a node, the total number

of nodes in the architecture will be A + A×B + 3×B^A + 1. In ANFIS, only the membership function parameters in Layer 1 and inputs weight in Layer 4 are to be predicted by training. Upon implication of the triangular membership function (*trimf*) which is represented by three parameters, we need to assess 3×B×A premise parameters in Layer 1 and A×B^A consequent weight parameters in Layer 4.

The structure of the ANFIS is automatically tuned by least-squares estimation and the back propagation algorithm. A fuzzy set A of a universe of discourse X is represented by a collection of ordered pairs of generic elements and its membership function *μA(x): X* tends to [0 1], which associates a number *μA(x)* to each element *x* of *X*. The fuzzy logic controller works on the basis of a set of control rules (called the fuzzy rules) among the linguistic variables. These fuzzy rules are represented in the form of conditional statements.

The basic structure of the pattern predictor model developed using ANFIS to predict the pattern of the flow regime consists of four important parts, namely, the fuzzification, knowledge base, artificial neural network, and de-fuzzification blocks, as shown in Scheme 3. The inputs to the ANFIS are the Zn^{2+} and PO_4^{3-}. These are fed to the fuzzification unit, which converts the binary data into linguistic variables. These in turn are given as inputs to the knowledge base block. The ANFIS tool in MATLAB 2017a developed 49 rules while training the neural network. The knowledge base block is connected to the artificial neural network block. A hybrid optimization algorithm is used to train the neural network and to select the proper set of rules for the knowledge base. To predict the emission intensity values at 457 nm, training is an important step in the selection of the proper rule base. Once the proper rule base is selected, the ANFIS model is ready to carry out prediction. The trained ANFIS was validated using 15% of the data. The output of the artificial neural network unit is given as input to the defuzzification unit, where the linguistic variables are converted back into numerical data in crisp form.

Reference:

1. A.Gogoi, S. Mukherjee, A. Ramesh and G. Das, *Rsc Advances*, 2015,**5(78),** 63634-63640.

2. A. Gogoi, S. Samanta and G. Das, *Sensors and Actuators B: Chemical*, 2014,**202,** 788-794.

3. Y. Xu, H. Wang, J. Zhao, X. Yang, M. Pei, G. Zhang, Y. Zhang and L.Lin, *Journal of Photochemistry and Photobiology A: Chemistry*, 2019,**383,** 112026.

4. B. Arvas, B. Ucar, T. Acar, M. B. Arvas, Y. Sahin, F. Aydogan, C.Yolacan, *Tetrahedron*, 2021,**88,** 132127.

5. Z. Y. Li, H. K. Su, K. Zhou, B. Z. Yang, T. Xiao, X. Q. Sun, J. Jiang and L. Wang, *Dyes and Pigments*, 2018,**149,** 921-926.

6. S. Wang, G.Men, L. Zhao, Q. Hou and S. Jiang, *Sensors and Actuators B: Chemical*,2010,**145(2),** 826-831.

7. J. C. Qin, L. Fan and Z. Y. Yang, *Sensors and Actuators B: Chemical*, 2016,**228,** 156-161.

8. M. Kumar, A. Kumar,M. K. Singh, S. K. Sahu and R. P. John, *Sensors and Actuators B: Chemical*, 2016,**241,** 1218-1223.

9. B. Das, A.Jana, A. D. Mahapatra, D. Chattopadhyay, A. Dhara, S. Mabhai and S. Dey, *Spectrochimica Acta Part A: Molecular and Biomolecular Spectroscopy*,2019,**212,** 222-231.

10. L. Fan, J. C.Qin, C. R.Li and Z. Y. Yang, *Spectrochimica Acta Part A: Molecular and Biomolecular Spectroscopy*, 2020,**236,** 118347.

11. B.Zha, S. Fang, H. Chen, H. Guo and F. Yang, *Spectrochimica Acta Part A: Molecular and Biomolecular Spectroscopy*, 2022,**269,** 120765.

12. J. Wang, Y. Li, E. Duah, S. Paruchuri, D. Zhou andY. Pang, *Journal of Materials Chemistry B*,2014,**2(14),** 2008-2012.

13. A.Pandey, S. K.Asthana, A. Prakash, J. K. Roy, I. Tiwari and K. K.Upadhyay,*Dalton Transactions*, 2019,**48(6),** 2068-2076.

14. H. Sun, Y.Jiang, J.Nie, J. Wei, B. Miao,Y. Zhao, L. Zhang and Z. Ni, *Materials Chemistry Frontiers*, 2021, **5(1),** 347-354.

15. R. Purkait, S. Dey and C.Sinhaa, *New Journal of Chemistry*, 2018,**42(20),** 16653-16665.

16. P. Das, S. S. Rajput, M. Das, S. Laha, I.Choudhuri, N. Bhattacharyya, A. Das,B. C. Samanta, M. M. Alam and T. Maity, *Journal of Photochemistry and Photobiology A: Chemistry*, 2022,**427,** 113817.

17. S. Chakraborty, S. Lohar, K. Dhara, R. Ghosh, S. Dam, E. Zangrando and P.Chattopadhyay, *Dalton Transactions*, 2020,**49(26),** 8991-9001.

18. L. Yan, Z.Li, Y. Xiong, X. Zhong, S. Peng and H.Li, *New Journal of Chemistry*, 2022,**46(27),** 12910-12917.

19. J. Jia and H.Zhao, *Organic Electronics*, 2019,**73,** 55-61.

20. M. Shyamal, P. Mazumdar, S. Maity, S. Samanta, G. P. Sahoo and A. Misra, *ACS Sensors*, 2016,**1(6),** 739-747.

21. B. Das, A. Ghosh, S. Yesmin, S. J. Abbas, M. Dolai, S. Mabhai, A. Jana, S. Dey and A. Misra, *Journal of Molecular Structure*, 2022,**1253,** 132295.

22. J. Wang, K. Hu, H. Wang, W. Sun, L. Han, L. Li and Y. Wei, *Journal of Molecular Structure*,2023,**1271,** 134085.

23. S. S.Samanta, P. K.Giri, S.Giri, A. Ghosh and A. Misra, *Journal of Molecular Structure*, 2023,134927.

24. S. N. K. Elmas, A. Karagoz, D. Aydin, F. N. Arslan, G. Sadi, I. Yilmaz*Talanta*, 2021,**226,** 122166.

25. S. Erdemir and O. Kocyigit, *Dyes and Pigments*, 2017,**145,** 72-79.

26. S. Erdemir, and S. Malkondu, *Dyes and Pigments*, 2019,**163,** 330-336.

27. A. Gul, M.Oguz, A. N. Kursunlu and M. Yilmaz, *Dyes and Pigments*, 2020,**176,** 108221.

28. M.Oguz, A. Oguz, A. A.Bhatti, A. Kocak and M. Yilmaz, *Journal of Molecular Liquids*, 2022,**348,** 118448.

29. B. Das, A. Ghosh, D. P.Dorairaj, M. Dolai, R. Karvembu, S. Mabhai, H. Im, S. Dey, A. Jana and A. Misra, *Journal of Molecular Liquids*,2022,**354,** 118824.

30. D. Aydin, S. Dinçkan, S. N. K. Elmas, T.Savran, F. N. Arslan and I. Yilmaz, *Food Chemistry*, 2021,**337,** 127659.

31. O. Alici and D. Aydin, *Journal of Photochemistry and Photobiology A: Chemistry*, 2021,**404,** 112876.

32. H. Kucukbasmaci and D. Aydin, *Journal of Photochemistry and Photobiology A: Chemistry*, 2023,**437,** 114460.

33. S. Wang, S. Liu, J. Zhang, X. Che, Z. Wang and D. Kong, *Spectrochimica Acta Part A: Molecular and Biomolecular Spectroscopy*, 2020,**228,** 117836.

34. Y. Li,C. Liao, S. Huang, H.Xu, B. Zheng, J. Du and D.Xiao, *RSC advances*, 2016,**6(30),** 25420-25426.

35. S. Erdemir, S.Malkondu and O. Kocyigit, *Luminescence*,2019,**34(1)**, 106-112.

36. D. Aydin and M. K. Alici, *Journal of Fluorescence*, 2021,**31,** 797-805.